Three-dimensional magnetic spin-echo small-angle neutron scattering and neutron depolarization: A comparison

M. Theo Rekveldt[a] and Niels H. van Dijk
Department of Radiation, Radionuclides and Reactors, Faculty of Applied Sciences, Delft University of Technology, 2629 JB Delft, The Netherlands

Serguei V. Grigoriev
Petersburg Nuclear Physics Institute, 188300 Gatchina, St-Petersburg District, Russia

Wicher H. Kraan and Wim G. Bouwman
Department of Radiation, Radionuclides and Reactors, Faculty of Applied Sciences, Delft University of Technology, 2629 JB Delft, The Netherlands

(Received 2 February 2006; accepted 16 April 2006; published online 7 July 2006)

The recently developed magnetic spin-echo small-angle neutron scattering (SANS) technique provides unique information about the distance correlation of the local vector magnetization as a function of the spin-echo length within a magnetic material. The technique probes the magnetic correlations on a length scale from 10 nm up to 10 μm within the bulk of a magnetic material by evaluating the Larmor precession of a polarized neutron beam in a spin-echo setup. The characteristics of the spin-echo SANS technique are discussed and compared to those of the more conventional neutron depolarization technique. Both of these techniques probe the average size of the magnetic inhomogeneities and the local magnetic texture. The magnetic spin-echo SANS technique gives information on the size distribution of these magnetic inhomogeneities perpendicular to the beam and, in principle, independent on the local magnetic induction. This information is not accessible by the neutron depolarization technique that gives the average size parallel to the beam multiplied with the square of the local magnetic induction. The basic possibilities of the magnetic spin-echo SANS technique are demonstrated by experiments on samples with a strong magnetic texture. © *2006 American Institute of Physics.*
[DOI: 10.1063/1.2204579]

I. INTRODUCTION

Neutron scattering techniques play an important role in the characterization of inhomogeneities in both magnetic and nonmagnetic materials. They cover a size range from atomic distances using normal diffraction,[1] to 1–100 nm using normal small-angle neutron scattering[2] (SANS), and, as demonstrated recently, extend to 10 nm–10 μm using spin-echo SANS (SESANS).[3] A related neutron technique, called neutron depolarization (ND),[4–6] also probes the size range from 0.1–10 μm but is only sensitive to magnetic inhomogeneities. The mentioned neutron techniques deliver their information, however, in different ways: diffraction and SANS give structural information from the scattered intensity as a function of the scattering angle. For SANS a size distribution of the inhomogeneities can be derived from the scattered intensity as a function of scattering angle. In the ND technique the total magnetic scattering cross section of a polarized neutron beam is derived from the change in polarization caused by the transmission of the beam through a magnetic sample. This change in polarization is a measure for the average size of the magnetic inhomogeneities. SESANS shows similarities with both the SANS and the ND techniques and measures the change in the polarization of a neutron beam, caused by the nuclear scattering in a nonmagnetic sample, in a spin-echo setup. As a result, the detected change in the polarization can be considered as a Fourier transform of the angular dependence of the scattered intensity. The change in the polarization as a function of the scanned spin-echo length reflects the spatial correlation function, which is related to the size distribution of the homogeneities.

Recently, an extension of the SESANS technique has been introduced, which also enables a study of magnetic inhomogeneities in *magnetic* samples.[7] In the magnetic SESANS technique the idea that the sample itself can function as a π flipper was exploited. As a consequence, the magnetic sample itself replaces the instrumental spin flipper necessary in any spin-echo setup to invert the phase accumulation. The principle was experimentally demonstrated for the first time in Ref. 7.

In this article we recognize that the spin flip properties of the sample depend on variations in the local magnetization vector within the sample. The resulting neutron scattering enables us to distinguish the SESANS correlation functions of the three magnetization components by various settings of the precession planes in the spin-echo setup. A possible π flip caused by magnetic scattering creates in some experimental geometries only a π phase change and in some other geometries an inversion of the phase accumulation, depend-

[a]Author to whom correspondence should be addressed; FAX: (31) 15-27-88303; electronic mail: m.t.rekveldt@tnw.tudelft.nl

ing on the orientation of the π rotation axis with respect to the precession plane. We will consider the possibilities of the magnetic SESANS technique in detail to generalize the one-dimensional nonmagnetic SESANS technique to the three-dimensional magnetic SESANS technique.

This article first describes in detail the principles of ND and SANS, then the principles of SESANS, and subsequently the characteristics of magnetic SESANS. The magnetic SESANS correlation function will be introduced and possible results compared with ND. Finally, new experiments using both ND and magnetic SESANS on magnetic foils with a strong magnetic texture are discussed.

II. NEUTRON DEPOLARIZATION AND SANS

Magnetically inhomogeneous systems, such as magnetic domain structures or local variations in the saturation magnetization can be studied by SANS (with or without polarized neutrons) to measure the magnetic correlation length in the range of 1–100 nm. For larger sizes, up to about 10 μm, three-dimensional neutron depolarization (3dND) can be used. For SANS with unpolarized neutrons the macroscopic magnetic differential scattering cross section $(d\Sigma/d\Omega)(\mathbf{Q})$ of a single magnetic domain is anisotropic. For a single magnetic domain with a uniform domain magnetization $\mathbf{M}$ with a normalized magnetization vector $\mathbf{m}=\mathbf{M}/M_s=(m_x,m_y,m_z)$ and an amplitude $|\mathbf{M}|=M_s$, the purely magnetic scattering is given by Refs. 1 and 2:

$$\left(\frac{d\Sigma}{d\Omega}\right)(\mathbf{Q}) = \frac{1}{V}\rho_m^2 V_p^2 |f_m(\mathbf{Q})|^2 |\mathbf{m}_\perp(\hat{\mathbf{Q}})|^2, \tag{1}$$

with

$$\mathbf{m}_\perp(\hat{\mathbf{Q}}_\perp) = \mathbf{m} - \hat{\mathbf{Q}}(\hat{\mathbf{Q}}\cdot\mathbf{m}) \text{ and } |\mathbf{m}_\perp(\hat{\mathbf{Q}})|^2 = 1 - (\hat{\mathbf{Q}}\cdot\mathbf{m})^2, \tag{2}$$

where $\mathbf{Q}=\mathbf{k}_{\text{out}}-\mathbf{k}_{\text{in}}$ is the wave vector transfer and $\hat{\mathbf{Q}}=\mathbf{Q}/Q$ is the unit vector of $\mathbf{Q}$ (with $|\mathbf{Q}|=Q$). $\mathbf{k}_{\text{in}}$ is the wave vector of the incoming neutron beam (oriented along x) and $\mathbf{k}_{\text{out}}$ the elastically scattered neutron beam. For elastic scattering the lengths of these wave vectors correspond to $|\mathbf{k}_{\text{in}}|=|\mathbf{k}_{\text{out}}|=k_0=2\pi/\lambda$, where λ is the neutron wave length. $V=St$ is the illuminated sample volume defined by the beam cross section S and the sample thickness t. $f_m(\mathbf{Q})$ is the form factor of the single magnetic domain with volume V_p. The magnetic scattering length density amounts to $\rho_m=N_0 b_m$, where N_0 is the number density of magnetic atoms and b_m the magnetic scattering length. The magnetic scattering length $b_m=(\gamma_n e/2h)(\mu_0 M_s/N_0)$, where γ_n is the gyromagnetic ratio of the neutron, e the electron charge, h Planck's constant, and μ_0 the permeability of vacuum. The prefactor of b_m amounts to $(\gamma_n e/2h)=2.313\times10^{14}\ \text{T}^{-1}\ \text{m}^{-2}$. In SANS experiments the magnetic scattering length is often expressed as $b_m=p_0\mu$, where $\mu=M_s/N_0$ is the average moment per atom within one domain and $p_0=2.699\ \text{fm}/\mu_B$ is a constant. The factor $|\mathbf{m}_\perp(\hat{\mathbf{Q}})|^2$ in Eqs. (1) and (2) expresses that there is no magnetic scattering for $\hat{\mathbf{Q}}\|\mathbf{m}$.

In the small-angle approximation ($Q_x\approx0$) the wave vector transfer $\mathbf{Q}$ is restricted to the yz plane and oriented perpendicular to the incident beam (oriented along x). Hence, using Eq. (2) the magnetic scattering from a single domain ($V=V_p$) is reduced to

$$\left(\frac{d\Sigma}{d\Omega}\right)(\mathbf{Q}) = V_p\rho_m^2|f_m(\mathbf{Q})|^2\left[1-\left(\frac{Q_y m_y + Q_z m_z}{Q}\right)^2\right]. \tag{3}$$

The total scattering cross section Σ is now obtained by

$$\Sigma = \int_{\Delta\Omega}\left(\frac{d\Sigma}{d\Omega}\right)(\mathbf{Q})d\Omega \cong \frac{1}{k_o^2}\int_{-\infty}^{\infty}\int_{-\infty}^{\infty}\left(\frac{d\Sigma}{d\Omega}\right)(\mathbf{Q})dQ_y dQ_z. \tag{4}$$

For isotropic scattering particles the form factor $f_m(\mathbf{Q})=f_m(Q)$ only depends on the size of the wave vector transfer. In this case the integral in the total scattering cross section Σ over Q_y and Q_z can be split up in an integral over Q and over the angle β in the yz plane, defined by $\mathbf{Q}=(0,Q_y,Q_z)=[0,Q\sin(\beta),Q\cos(\beta)]$. Then using Eqs. (1) and (3) in Eq. (4), we get

$$\begin{aligned}\Sigma &= \frac{V_p\rho_m^2}{k_o^2}\left(\int_0^\infty |f_m(Q)|^2 Q dQ\right)\left(\int_0^{2\pi} d\beta|\mathbf{m}_\perp(\beta)|^2\right)\\ &= \rho_m^2\lambda^2\delta_\|\left(\frac{1}{2\pi}\int_0^{2\pi}d\beta|\mathbf{m}_\perp(\beta)|^2\right) = \rho_m^2\lambda^2\delta_\|\left(\frac{1+\langle m_x^2\rangle}{2}\right),\end{aligned} \tag{5}$$

$$\text{with } \delta_\| = \frac{V_p}{2\pi}\int_0^\infty |f_m(Q)|^2 Q dQ. \tag{6}$$

The latter equation can simply be proven for a spherical or cylindrical domain and is generally true also for other shapes with random orientations.

The number of scattering events due to magnetic small-angle scattering during the transmission of the sample amounts to $\Sigma V/S=\Sigma t\equiv\Sigma\delta_\|$, where t is the effective sample thickness that corresponds to $\delta_\|$ for a single domain. It is interesting to note that the total scattering power $\Sigma\delta_\|$ is independent of the dimensions of the domain perpendicular to the beam, and therefore Eq. (5) is also valid for a wide beam transmitting a large number of parallel domains. The factor $(1+\langle m_k^2\rangle)/2$ is the result of the integration over Q_y and Q_z perpendicular to the transmission direction x and expresses that there is no scattering in the direction of the magnetization. The property of having no magnetic scattering for $\mathbf{m}\|\hat{\mathbf{Q}}$ originates from Maxwell's law $\nabla\cdot\mathbf{B}=0$ and is often used to separate the magnetic and nuclear scatterings. When the orientation of the magnetization $\mathbf{m}$ is known from an applied magnetic field or a strong magnetic texture, then the anisotropy in the scattered intensity allows for a direct determination of the purely magnetic scattering. For a purely magnetic scattering of a polarized neutron beam with an initial polarization $\mathbf{P}_0$, the polarization of the scattered neutrons $\mathbf{P}_s(\mathbf{Q})$ is given by[8]

$$\mathbf{P}_s(\mathbf{Q}) = \frac{2(\mathbf{m}_\perp(\hat{\mathbf{Q}})\cdot\mathbf{P}_0)\mathbf{m}_\perp(\hat{\mathbf{Q}})}{|\mathbf{m}_\perp(\hat{\mathbf{Q}})|^2} - \mathbf{P}_0. \tag{7}$$

This equation expresses that the polarization of the scattered neutrons is obtained by flipping the initial polarization $\mathbf{P}_0$ over π around the local magnetization direction $\mathbf{m}$.

For large magnetic inhomogeneities (micron size) the magnetic form factor $f_m(\mathbf{Q})$ indicates that the dominant scattering angles are so small that it cannot be resolved in a SANS experiment. In this case we can use the 3dND technique to analyze the change in the polarization from the added intensity of the transmitted and scattered beams. According to Eq. (7) the magnetic domain scattering causes a change in the polarization of the neutron beam that can be used as a measure of the magnetic domain size with Eq. (5), as the total scattering power Σt gives a measure of $\delta_\parallel$. This can be understood from the fact that the transmitted polarization is composed of two terms. The first term is the unscattered transmitted beam that did not change its polarization, and the second term is the scattered fraction of the beam that changed its polarization according to Eq. (7). In the weak-scattering approximation ($\Sigma t \ll 1$) this leads to

$$\mathbf{P} = \mathbf{P}_0(1-\Sigma t) + \frac{t}{k_o^2}\int_{-\infty}^{\infty}\int_{-\infty}^{\infty}\mathbf{P}_s(\mathbf{Q})\left(\frac{d\Sigma}{d\Omega}\right)(\mathbf{Q})dQ_y dQ_z, \tag{8}$$

where $t=\delta_\parallel$ for a single domain. This result can easily be generated for a strong scattering.[3,10,11] Combining Eqs. (5) and (7) we find for the change in the polarization $\Delta\mathbf{P}$ for a single domain ($V=V_p$):

$$\Delta\mathbf{P} = \mathbf{P}_0 - \mathbf{P} = \mathbf{P}_0\Sigma t - \frac{t}{k_o^2}\int_{-\infty}^{\infty}\int_{-\infty}^{\infty}\mathbf{P}_s(\mathbf{Q})\left(\frac{d\Sigma}{d\Omega}\right) \times(\mathbf{Q})dQ_y dQ_z. \tag{9}$$

Substituting Eq. (7) in (9) gives

$$\begin{aligned}\Delta\mathbf{P} &= \mathbf{P}_0\Sigma t - \frac{t}{k_o^2}\int_{-\infty}^{\infty}\int_{-\infty}^{\infty}\frac{2(\mathbf{m}_\perp(\hat{\mathbf{Q}})\cdot\mathbf{P}_0)\mathbf{m}_\perp(\hat{\mathbf{Q}}) - \mathbf{P}_0|\mathbf{m}_\perp(\hat{\mathbf{Q}})|^2}{|\mathbf{m}_\perp(\hat{\mathbf{Q}})|^2}\left(\frac{d\Sigma}{d\Omega}\right)(\mathbf{Q})dQ_y dQ_z \\ &= 2\mathbf{P}_0\Sigma t - \frac{t}{k_o^2}\int_{-\infty}^{\infty}\int_{-\infty}^{\infty}\frac{2(\mathbf{m}_\perp(\hat{\mathbf{Q}})\cdot\mathbf{P}_0)\mathbf{m}_\perp(\hat{\mathbf{Q}})}{|\mathbf{m}_\perp(\hat{\mathbf{Q}})|^2}\left(\frac{d\Sigma}{d\Omega}\right)(\mathbf{Q})dQ_y dQ_z.\end{aligned} \tag{10}$$

Substituting Eq. (1) in (10) yields

$$\begin{aligned}\Delta\mathbf{P} &= 2\mathbf{P}_0\Sigma t - \frac{2Vt\rho_m^2}{k_o^2}\int_{-\infty}^{\infty}\int_{-\infty}^{\infty}(\mathbf{m}_\perp(\hat{\mathbf{Q}})\cdot\mathbf{P}_0)\mathbf{m}_\perp(\hat{\mathbf{Q}})|f_m(\mathbf{Q})|^2 dQ_y dQ_z \\ &= 2\mathbf{P}_0\Sigma t - \frac{2Vt\rho_m^2}{k_o^2}\left[\int_0^{\infty}|f_m(Q)|^2 Q dQ\right]\left[\int_0^{2\pi}(\mathbf{m}_\perp(\beta)\cdot\mathbf{P}_0)\mathbf{m}_\perp(\beta)d\beta\right] \\ &= 2\mathbf{P}_0\Sigma t - \frac{\Sigma t}{\left(\int_0^{2\pi}|\mathbf{m}_\perp(\beta)|^2 d\beta\right)}\left[\int_0^{2\pi}(\mathbf{m}_\perp(\beta)\cdot\mathbf{P}_0)\mathbf{m}_\perp(\beta)d\beta\right] \\ &= 2\Sigma t\left\{\mathbf{P}_0 - \frac{2}{1+\langle m_x^2\rangle}\left[\int_0^{2\pi}(\mathbf{m}_\perp(\beta)\cdot\mathbf{P}_0)\mathbf{m}_\perp(\beta)d\beta\right]\right\}.\end{aligned} \tag{11}$$

For a sample with many domains parallel in the beam with $\langle m_x\rangle=\langle m_y\rangle=\langle m_z\rangle=0$ this leads to

$$\begin{aligned}\Delta\mathbf{P} = 2\Sigma t\Bigg\{&\left(1-\frac{2\langle m_x^2\rangle}{1+\langle m_x^2\rangle}\right)P_{0x}\hat{\mathbf{i}}_x \\ &+\left[1-\frac{3\langle m_y^2\rangle+\langle m_z^2\rangle}{4(1+\langle m_x^2\rangle)}\right]P_{0y}\hat{\mathbf{i}}_y \\ &+\left[1-\frac{\langle m_y^2\rangle+3\langle m_z^2\rangle}{4(1+\langle m_x^2\rangle)}\right]P_{0z}\hat{\mathbf{i}}_z\Bigg\}\end{aligned} \tag{12}$$

In terms of the neutron depolarization, this corresponds to[9]

$$\frac{\Delta P_{ii}}{P_{0i}} \equiv 1 - \frac{P_{si}}{P_{0i}} \equiv c(\xi-\alpha_{ii})t = 2\Sigma t(1-\gamma_i) \tag{13}$$

with

$$\gamma_x = \frac{2\langle m_x^2\rangle}{1+\langle m_x^2\rangle}, \quad \gamma_y = \frac{3\langle m_y^2\rangle+\langle m_z^2\rangle}{4(1+\langle m_x^2\rangle)}, \quad \gamma_z = \frac{\langle m_y^2\rangle+3\langle m_z^2\rangle}{4(1+\langle m_x^2\rangle)}, \tag{14}$$

where α_{ii} is the correlation function of the variation in the magnetic induction B_i along direction i. The correlation function of the variation in the vector $\mathbf{B}$ corresponds to $\xi=\alpha_{xx}+\alpha_{yy}+\omega_{zz}$, and the magnetic texture parameters are defined as $\gamma_i=\omega_{ii}/\xi$. The constant c amounts to $c=(\gamma_L/\nu)^2=(m_n/h)^2\gamma_L^2\lambda^2=(2.146\times10^{29})\lambda^2\ \mathrm{m}^{-2}$, where $\nu=h/m_n\lambda$ is the neutron velocity, $\gamma_L=\gamma_n e/m_n=1.8325\times10^8\ \mathrm{s}^{-1}\ \mathrm{T}^{-1}$ the Larmor constant, m_n the neutron mass, h Planck's constant, and e the electron charge.

The scattering length density ρ_m in a magnetic field of $B=\mu_0 M_s$, produced by a homogeneously magnetized domain in the absence of stray fields, is directly related to the Larmor precession frequency ω_L. The Larmor precession frequency

amounts to $\omega_L = \gamma_L B$. For $B = \mu_0 M_s$ the Larmor frequency is related to the magnetic scattering length density ρ_m by

$$\omega_L = \left(\frac{2h}{m_n}\right)\left(\frac{B}{\mu_0 M_s}\right)\rho_m \equiv \left(\frac{2h}{m_n}\right)\rho_m. \tag{15}$$

The precession in a single domain $\Delta\varphi = \lambda\rho_m\delta_\parallel$ is obtained from $\Delta\varphi = \omega_L\tau$, where the transmission time amounts to $\tau = \delta_\parallel/\nu$ with a neutron velocity $\nu = h/m_n\lambda$. It is worthwile to note that the precession mentioned here has nothing to do with the polarization change by scattering as introduced in Eq. (7). The precession angle reflects the phase change of the neutron wave over the particle and is therefore proportional to the particle size $\delta_\parallel$.

The depolarization of the beam caused by the sample directly depends on the domain size $\delta_\parallel$. When the magnetic sample thickness corresponds to $t = N\delta_\parallel$ with N magnetic domains, then the average magnetic texture components $\langle m_i^2\rangle$ $(i = x, y, z)$ can be determined from the 3dND experiment. More details about this method were published elsewhere.[4–6]

The basic difference between SANS and 3dND is that in scattering one determines the dimensions perpendicular to the transmission direction $(\delta_\perp)$ and, in principle, independent of the local magnetic induction, while in depolarization one determines the dimension parallel to the transmission direction $(\delta_\parallel)$ in the product with the square of the local magnetic induction. The quantity $\delta_\perp$ is determined from the Q dependence of the scattered intensity, while $\delta_\parallel$ is determined from the total magnetic cross section. In this sense both techniques are fully complementary.

III. SESANS (NUCLEAR SCATTERING)

In SESANS the polarization analysis is only used to characterize the relatively small scattering angle. The method is based on the different path lengths a neutron experiences by traveling through a precession region with parallel boundaries inclined by an angle θ_0 with the neutron transmission direction, as sketched in Fig. 1. After the transmission through two of such regions with opposite precession directions with a scattering sample in between, the final beam is composed of a transmitted and a scattered part. The polarization of the scattered part of this neutron beam can be written as[3,10,11]

$$\frac{P(Z)}{P_0} = \cos\varphi = \cos(ZQ_z), \tag{16}$$

where P_0 is the incident neutron beam polarization in a selected direction in the precession plane and $P(Z)$ is the projected polarization of the scattered beam on the analyzing direction. In principle, we are able to choose the precession axis in any direction we want, independent of the direction in which the spin-echo length Z is varied using polarization rotators Pr(i) and Pr(j) sandwiched around the sample. For the moment we choose the z direction as the precession axis. The quantity Z and the component Q_z of the momentum transfer in the sample between the precession devices can be derived from the geometry[10]

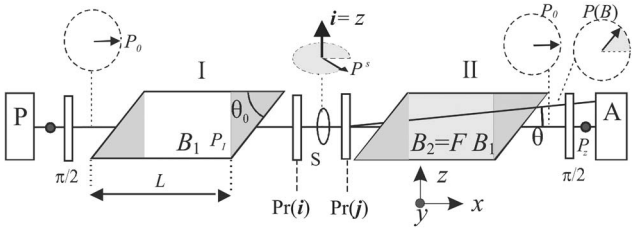

FIG. 1. Principles of the spin-echo setup for small-angle neutron scattering. A neutron beam passes from left to right through the setup. After being polarized in P, its polarization is rotated over $\pi/2$ to the (x,z) precession plane. Then the polarization precesses in the precession regions I and II in parallel or opposite directions depending on the sign of F of the instrumental flipper expressed in $B_2 = \mathrm{F}\ B_1$. Sandwiched around the sample two polarization rotators [Pr(i) and Pr(j)] are mounted to change the precession axes at the sample into the x, y, or z direction and rotate the direction j back to the initial precession direction. After another rotation over $\pi/2$, the neutrons pass through the analyzer A, and are detected. The inclined precession faces, which make an angle θ_0 with the x axis, cause the precession angle in regions I and II to be strongly dependent on the incident angle of the neutron. In the absence of a scattering sample S the two precession angles cancel each other if $F = -1$. However, even a small scattering angle disturbs the echo, which can be detected and analyzed from the final polarization. It should be noted that the technique is insensitive to the divergence of the incoming neutron beam. Only the shadowed areas in the precession regions cause the inclination effect, while the remaining parts do not contribute.

$$Z = \frac{c\lambda^2 L\langle\cot(\theta_0)\rangle_\alpha}{2\pi}B \text{ and } Q_z = \frac{4\pi\sin(\theta)}{\lambda} \approx \frac{2\pi\theta_s}{\lambda}, \tag{17}$$

where $\cot(\theta_0)$ has been averaged over the divergence α of the neutron beam. The spin-echo length Z is an instrumental quantity that corresponds to the probed correlation length in the illuminated sample volume. In the small-angle approximation $\sin(\theta) \approx \theta$, where θ is the Bragg angle. The scattering angle amounts to $\theta_s = 2\theta$.

When we also consider the nonscattered neutrons that pass through the setup, the measured polarization of the transmitted beam including multiple scattering effects can be written as[3,10,11]

$$\frac{P(Z)}{P_0} = \exp[-\Sigma t(1 - G(Z))]. \tag{18}$$

This result is exact with no weak-scattering approximation and is a generalization of the result obtained for the weak-scattering approximation $(\Sigma t \ll 1)$:

$$\frac{P(Z)}{P_0} = 1 - \Sigma t + \Sigma t G(Z), \tag{19}$$

where Σt is the fraction of elastically scattered neutrons. So Eq. (18) is valid also in the case of strong scattering. The SESANS correlation function $G(Z)$ is defined as

$$G(Z) = \frac{1}{\Sigma k_0^2}\int_{-\infty}^{\infty}\int_{-\infty}^{\infty}\left(\frac{d\Sigma}{d\Omega}\right)(\mathbf{Q})\cos(ZQ_z)dQ_y dQ_z, \tag{20}$$

where $k_0 = |\mathbf{k}_{\mathrm{in}}| = |\mathbf{k}_{\mathrm{out}}|$ is the magnitude of the wave vector of the incident and of elastically scattered beams.

Recently, the SESANS correlation function $G(Z)$ has been identified as a projection of the correlation function $\gamma(\mathbf{r}) = \gamma(x,y,z)$ for the variation in the nuclear scattering length density[12] along the beam direction:

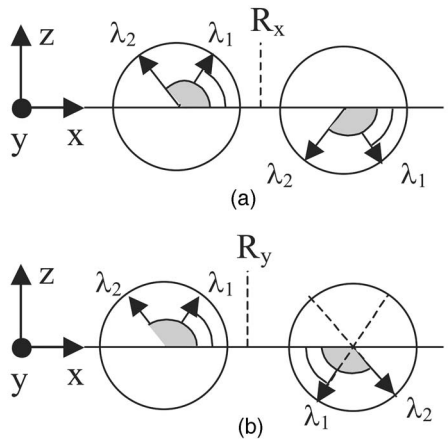

FIG. 2. (a) Effect of a π flip around an axis in the precession plane. Realizing that before and after the flip the precession direction remains the same because the field has not changed, the precession phase of the neutrons with λ_1, which were behind in phase compared to λ_2 before flipping, has an advanced phase after flipping. (b) A π flip around the precession axis y itself creates only a π phase shift.

$$G(Z) = \int_{-\infty}^{\infty} dx \gamma(x,0,Z) \Big/ \int_{-\infty}^{\infty} dx \gamma(x,0,0) \tag{21}$$

with

$$\gamma(x,y,z) = \frac{1}{V} \int \int_V \int dx' dy' dz' \times \Delta\rho(x',y',z') \Delta\rho(x'+x, y'+y, z'+z), \tag{22}$$

where $\Delta\rho(x,y,z) = \rho(x,y,z) - \langle\rho\rangle$. The definition of $\gamma(x,y,z)$ in Eq. (22) leads to a value of $\gamma(0,0,0) = \langle\Delta\rho^2\rangle$, where $\langle\Delta\rho^2\rangle$ is the volume average of the square variation in the scattering length density. The normalized correlation function now corresponds to $\gamma'(x,y,z) = \gamma(x,y,z)/\gamma(0,0,0) = \gamma(x,y,z)/\langle\Delta\rho^2\rangle$. Using these equations, model calculations of $G(Z)$ can be done analytically for some standard particle shapes. One finds $G(Z)=1$ for $Z=0$ and $G(Z)=0$ for $Z\to\infty$. The total scattering cross section Σ amounts to

$$\Sigma = \lambda^2 \int_{-\infty}^{\infty} dx \gamma(x,0,0) \equiv 2\lambda^2 \gamma(0,0,0) \zeta_{\|} = \lambda^2 \langle\Delta\rho^2\rangle \delta_{\|} \tag{23}$$

with

$$\zeta_{\|} = \frac{1}{2} \frac{\int_{-\infty}^{\infty} \gamma(x,0,0) dx}{\gamma(0,0,0)} = \frac{1}{2} \int_{-\infty}^{\infty} \gamma'(x,0,0) dx, \tag{24}$$

where $\zeta_{\|}$ is the nuclear correlation length for the variation in the scattering length density along the beam. The effective size of the inhomogeneities along the neutron beam corresponds to $\delta_{\|} = 2\zeta_{\|}$. The average number of scattering events amounts to $\Sigma t = \lambda^2 \langle\Delta\rho^2\rangle \delta_{\|} t$.

The essential property of the SESANS method is that the phase accumulation of the neutron spins reverses between the precession devices. This can only be achieved by a sudden change in the field direction or by a π flip around an axis that is in the precession plane of the polarization. This can be understood from Fig. 2 (left) where we sketch the spin directions of neutrons with wavelengths λ_1 and λ_2 with accumulated phases in the first precession device, proportional to the wavelength, before and after the π flip in the precession plane. A π flip around an axis perpendicular to the precession plane does not change the sign of phase accumulation, but only changes the precession phase by π.

IV. CHARACTERISTICS OF MAGNETIC SESANS

Consider now the case that we have an unmagnetized magnetic sample in the SESANS setup. The average polarization of the scattered neutrons in this case at the wave vector transfer $\mathbf{Q}$ can be derived from Eq. (7) by skipping all linear terms in $m_{\perp i}$ and is given by

$$\mathbf{P}_s(\mathbf{Q}) = \left\{ \frac{2[m_{\perp x}(\hat{\mathbf{Q}})]^2}{|\mathbf{m}_{\perp}(\mathbf{Q})|^2} - 1 \right\} P_{0x} \hat{\mathbf{i}}_x + \left\{ \frac{2[m_{\perp y}(\hat{\mathbf{Q}})]^2}{|\mathbf{m}_{\perp}(\mathbf{Q})|^2} - 1 \right\} \times P_{0y} \hat{\mathbf{i}}_y + \left\{ \frac{2[m_{\perp z}(\hat{\mathbf{Q}})]^2}{|\mathbf{m}_{\perp}(\mathbf{Q})|^2} - 1 \right\} P_{0z} \hat{\mathbf{i}}_z. \tag{25}$$

This formula shows that in an unmagnetized sample ($\langle m_x\rangle = \langle m_y\rangle = \langle m_z\rangle = 0$), the polarization of the scattered neutrons does change its direction with the sign and amplitude of its components. Dependent on the magnitude of the magnetization components, a spin flip may occur that changes the phase accumulation. In textured materials where one of the magnetization components is smaller than the others, we see from Eq. (25) that a spin flip occurs in one or two polarization components, changing also the phase accumulation in the spin echo.

We will now evaluate Eq. (25), assuming that the $\mathbf{P}_0$ components in the precession plane possess a precession phase φ at the sample position. For example, in the xy precession plane we find

$$P_{0x} = P_0 \sin(\varphi), \qquad P_{0y} = P_0 \cos(\varphi). \tag{26}$$

In the second arm of the spin-echo setup another precession angle φ is subtracted with an instrumental spin flip ($F=-1$) or added without an instrumental spin flip ($F=1$). These two settings for the instrumental spin flip in the second spin-echo

arm probe the non-spin-flip (NSF) and the spin-flip (SF) scattering in the sample. At the detector we analyze the y component of the polarization resulting for the unscattered neutrons in

$$P_{0d|F} = P_{0y}\cos(\varphi) - FP_{0x}\sin(\varphi),$$

$$P_{0d|F=-1} = P_0[\cos^2(\varphi) + \sin^2(\varphi)] = P_0,$$

$$P_{0d|F=+1} = P_0[\cos^2(\varphi) - \sin^2(\varphi)] = P_0\cos 2\varphi. \tag{27}$$

For the polarization of the scattered neutrons with the wave vector transfer $\mathbf{Q}$ as given in Eq. (25), we obtain the following in a similar way:

$$\begin{aligned} P_{sd}(\mathbf{Q}) &= (P_{sy}(\mathbf{Q})\cos\varphi - FP_{sx}(\mathbf{Q})\sin\varphi) \\ &= P_{0y}\left(\frac{2m_{y\perp}^2(\hat{\mathbf{Q}})}{|\mathbf{m}_\perp(\hat{\mathbf{Q}})|^2} - 1\right)\cos\varphi - FP_{0x}\left(\frac{2m_{\perp x}^2(\hat{\mathbf{Q}})}{|\mathbf{m}_\perp(\hat{\mathbf{Q}})|^2} - 1\right)\sin\varphi \\ &= P_0\left(\frac{2m_{y\perp}^2(\hat{\mathbf{Q}})}{|\mathbf{m}_\perp(\hat{\mathbf{Q}})|^2} - 1\right)\cos^2\varphi - FP_0\left(\frac{2m_{\perp x}^2(\hat{\mathbf{Q}})}{|\mathbf{m}_\perp(\hat{\mathbf{Q}})|^2} - 1\right)\sin^2\varphi \\ &= P_0\left(-\frac{m_{\perp z}^2(\hat{\mathbf{Q}})}{|\mathbf{m}_\perp(\hat{\mathbf{Q}})|^2}\cos 2\varphi + \frac{(m_{\perp y}^2(\hat{\mathbf{Q}}) - m_{\perp x}^2(\hat{\mathbf{Q}}))}{|\mathbf{m}_\perp(\hat{\mathbf{Q}})|^2}\right) \quad \text{if } F = 1 \\ &= P_0\left(-\frac{m_{\perp z}^2(\hat{\mathbf{Q}})}{|\mathbf{m}_\perp(\hat{\mathbf{Q}})|^2} + \frac{(m_{\perp y}^2(\hat{\mathbf{Q}}) - m_{\perp x}^2(\hat{\mathbf{Q}}))}{|\mathbf{m}_\perp(\hat{\mathbf{Q}})|^2}\cos 2\varphi\right) \quad \text{if } F = -1. \end{aligned} \tag{28}$$

More generally, for a precession axis along $i=x,y,z$ we obtain

$$P_{si|F=-1}(\hat{\mathbf{Q}}) = P_0[A_{i|-}(\hat{\mathbf{Q}}) + A_{i|+}(\hat{\mathbf{Q}})\cos 2\varphi] \simeq P_0A_{i|-}(\hat{\mathbf{Q}}),$$
$$P_{si|F=+1}(\hat{\mathbf{Q}}) = P_0[A_{i|-}(\hat{\mathbf{Q}})\cos 2\varphi + A_{i|+}(\hat{\mathbf{Q}})] \simeq P_0A_{i|+}(\hat{\mathbf{Q}}). \tag{29}$$

Because φ is proportional to the neutron wavelength λ, the spread in the wavelength of the beam leads to an averaging out of the $\cos(2\varphi)$ term for large precession angles $[\langle\cos(2\varphi)\rangle \approx 0$ for $\varphi \gg 0]$ resulting in

$$A_{i|-}(\hat{\mathbf{Q}}) = \frac{-m_{i\perp}^2(\hat{\mathbf{Q}})}{|\mathbf{m}_\perp(\hat{\mathbf{Q}})|^2},$$

$$A_{i|+}(\hat{\mathbf{Q}}) = \frac{m_{j\perp}^2(\hat{\mathbf{Q}}) - m_{k\perp}^2(\hat{\mathbf{Q}})}{|\mathbf{m}_\perp(\hat{\mathbf{Q}})|^2}, \tag{30}$$

where $i \neq j \neq k$ and j corresponds to a direction in the precession plane about which the instrumental π rotation takes place [the y axis in Eq. (28)]. Equation (30) can be rewritten in the more general form

$$A_{iF}(\hat{\mathbf{Q}}) = \frac{1-F}{2}\left[\frac{-m_{i\perp}^2(\hat{\mathbf{Q}})}{|\mathbf{m}_\perp(\hat{\mathbf{Q}})|^2}\right] + \frac{1+F}{2}\left[\frac{m_{j\perp}^2(\hat{\mathbf{Q}}) - m_{k\perp}^2(\hat{\mathbf{Q}})}{|\mathbf{m}_\perp(\hat{\mathbf{Q}})|^2}\right], \tag{31}$$

with i, j, and k as described above. The flip parameter F indicates an instrumental spin flip for $F=-1$ and no instrumental spin flip for $F=+1$.

Equation (31) reflects the sensitivity of the measured amplitudes for the spin flip occurring in the instrumental flipper and the spin flip caused by the magnetic scattering. For a selected precession plane a measurement with and without an instrumental spin flip probes the magnetic texture of the sample from the amplitude of the measured signals.

To probe all the mentioned possibilities it is required to change the precession planes at the sample position. In the present setup we realized the precession xy and zx planes by introducing simple polarization rotators in front of and behind the sample position (see Fig. 1).

V. MAGNETIC SESANS CORRELATION FUNCTION

It is clear that the difference in sensitivity of the spin-echo signal on components of the variation in the local vector magnetization, summarized in Eq. (31), has consequences for the magnetic correlations measured in a system with both nuclear and magnetic inhomogeneities. We therefore consider, in analogy with the nuclear SESANS correlation function in Eqs. (19) and (20), a magnetic SESANS correlation function $G_{iF}(Z)$. The measured polarization of the transmitted beam can be written as

$$\frac{P_{iF}(Z)}{P_0} = \exp[-\Sigma t(1 - G_{iF}(Z))]. \tag{32}$$

This is the generalization of the result obtained for the weak-scattering approximation:

$$\frac{P_{iF}(Z)}{P_0} = (1 - \Sigma t) + \Sigma tG_{iF}(Z) = 1 - \Sigma t[1 - G_{iF}(Z)], \tag{33}$$

where the magnetic SESANS correlation function $G_{iF}(Z)$ corresponds to

$$G_{iF}(Z) = \frac{1}{\Sigma k_0^2}\int_{-\infty}^{\infty}\int_{-\infty}^{\infty} A_{iF}(\hat{\mathbf{Q}})\left(\frac{d\Sigma}{d\Omega}\right)(\mathbf{Q})\cos(ZQ_z)dQ_y dQ_z$$
$$= \frac{1}{\Sigma k_0^2}\int_{-\infty}^{\infty}\int_{-\infty}^{\infty}\left\{\frac{1-F}{2}\left[\frac{-m_{i\perp}^2(\hat{\mathbf{Q}})}{|\mathbf{m}_\perp(\hat{\mathbf{Q}})|^2}\right] + \frac{1+F}{2}\left[\frac{m_{j\perp}^2(\hat{\mathbf{Q}}) - m_{k\perp}^2(\hat{\mathbf{Q}})}{|\mathbf{m}_\perp(\hat{\mathbf{Q}})|^2}\right]\right\} \times \frac{V_p^2}{V}\rho_m^2|f_m(\mathbf{Q})|^2|\mathbf{m}_\perp(\hat{\mathbf{Q}})|^2\cos(ZQ_z)dQ_y dQ_z$$
$$= \frac{1}{\Sigma k_0^2}\frac{V_p^2}{V}\rho_m^2\left\{-\left(\frac{1-F}{2}\right)\int_{-\infty}^{\infty}\int_{-\infty}^{\infty}|f_m(\mathbf{Q})|^2\mathbf{m}_{i\perp}^2(\hat{\mathbf{Q}})\cos(ZQ_z)dQ_y dQ_z\right.$$
$$\left. + \left(\frac{1+F}{2}\right)\int_{-\infty}^{\infty}\int_{-\infty}^{\infty}|f_m(\mathbf{Q})|^2[m_{j\perp}^2(\hat{\mathbf{Q}}) - m_{k\perp}^2(\hat{\mathbf{Q}})]\cos(ZQ_z)dQ_y dQ_z\right\}. \quad (34)$$

In real space the magnetic SESANS correlation function $G_{iF}(Z)$ can be translated to

$$G_{iF}(Z) = \frac{-[(1-F)/2]\int_{-\infty}^{\infty}dx\Gamma_{ii}(x,0,Z) + [(1+F)/2]\int_{-\infty}^{\infty}dx[\Gamma_{jj}(x,0,Z) - \Gamma_{kk}(x,0,Z)]}{\Sigma_i\int_{-\infty}^{\infty}dx\Gamma_{ii}(x,0,0)}, \quad (35)$$

where $i \neq j \neq k$ and k corresponds to a direction that makes $\pi/2$ with the symmetry axis between the two precession regions. Although Eq. (35) has been derived for a nonmagnetized sample, it can be shown that it is also valid for a magnetized sample. In the latter case a term with $\sin(2\varphi)$ enters in Eq. (28) and (29) and that averages out to zero at a large precession angle φ. The correlation length determined with Eq. (35) is, in principle, independent of ρ_m that contains the local magnetic induction B.

The magnetic correlation function $\Gamma_{ij}(\mathbf{r}) = \Gamma_{ij}(x,y,z)$ for the variation in the vector components of the scattering length density $\rho_B = (\rho_m/\mu_0 M_s)\mathbf{B}$ is defined as

$$\Gamma_{ij}(x,y,z) = \langle\Delta\rho_{B,i}(0,0,0)\Delta\rho_{B,j}(x,y,z)\rangle$$
$$= \left(\frac{\rho_m}{\mu_0 M_s}\right)^2\langle\Delta B_i(0,0,0)\Delta B_j(x,y,z)\rangle$$
$$= \frac{1}{V}\left(\frac{\rho_m}{\mu_0 M_s}\right)^2\int\int_V\int dx'dy'dz'$$
$$\times\Delta B_i(x',y',z')\Delta B_j(x'+x,y'+y,z'+z), \quad (36)$$

where $\Gamma_{ij}(x,y,z)$ generally forms a 3×3 matrix. The definition of $\Gamma_{ij}(x,y,z)$ in Eq. (36) leads to a value of $\Gamma_{ij}(0,0,0) = (\rho_m/\mu_0 M_s)^2\langle\Delta B_i\Delta B_j\rangle$, where $\langle\Delta B_i\Delta B_j\rangle$ is the volume average of the variation in $\Delta B_i\Delta B_j$. The normalized correlation function now corresponds to $\Gamma'_{ij}(x,y,z) = \Gamma_{ij}(x,y,z)/\Gamma_{ij}(0,0,0) = \Gamma_{ij}(x,y,z)/[(\rho_m/\mu_0 M_s)^2\langle\Delta B_i\Delta B_j\rangle]$. For an unmagnetized sample $\langle\mathbf{B}\rangle = 0$, and therefore $\Delta B_i = B_i$. For sample geometries that do not produce magnetic stray fields, the magnetic induction is directly related to the magnetization by $\mathbf{B} = \mu_0\mathbf{M} = \mu_0 M_s\mathbf{m}$.

The magnetic correlation function $\Gamma_{ij}(x,y,z)$ can be linked directly to the correlation parameters α_{ij} and $\xi = \alpha_{xx} + \alpha_{yy} + \alpha_{zz}$ probed in a neutron depolarization experiment:

$$\alpha_{ij} = \frac{1}{V}\int\int_V\int\int_{-\infty}^{\infty}dx'dy'dz'dx$$
$$\times\Delta B_i(x',y',z')\Delta B_j(x'+x,y',z')$$
$$= \left(\frac{\rho_m}{\mu_0 M_s}\right)^{-2}\int_{-\infty}^{\infty}dx\Gamma_{ij}(x,0,0),$$
$$\xi = \frac{1}{V}\int\int_V\int\int_{-\infty}^{\infty}dx'dy'dz'dx$$
$$\times\Delta\mathbf{B}(x',y',z')\cdot\Delta\mathbf{B}(x'+x,y',z')$$
$$= \left(\frac{\rho_m}{\mu_0 M_s}\right)^{-2}\left[\int_{-\infty}^{\infty}dx\Gamma_{xx}(x,0,0) + \int_{-\infty}^{\infty}dx\Gamma_{yy}(x,0,0)\right.$$
$$\left. + \int_{-\infty}^{\infty}dx\Gamma_{zz}(x,0,0)\right], \quad (37)$$

where α_{ij} and ξ are in units of mT^2. For random domain orientations $\alpha_{ij} = 0$ for $i \neq j$. The total scattering cross section for the unpolarized neutron beam can also be written in terms of the correlation functions and results in similar expressions as given already in Eq. (5):

$$\Sigma = \lambda^2\left[\int_{-\infty}^{\infty}dx\Gamma_{xx}(x,0,0) + \int_{-\infty}^{\infty}dx\Gamma_{yy}(x,0,0)\right.$$
$$\left. + \int_{-\infty}^{\infty}dx\Gamma_{zz}(x,0,0)\right]$$
$$= \lambda^2\left(\frac{\rho_m}{\mu_0 M_s}\right)^2\xi \equiv 2\lambda^2[\Gamma_{xx}(0,0,0) + \Gamma_{xx}(0,0,0)$$
$$+ \Gamma_{xx}(0,0,0)]\zeta_\parallel = \lambda^2\frac{\langle|\Delta\mathbf{B}|^2\rangle}{(\mu_0 M_s)^2}\rho_m^2\delta_\parallel. \quad (38)$$

VI. COMPARISON BETWEEN MAGNETIC SESANS AND 3dND

With 3dND the correlation parameters α_{ij} $(i = x,y,z)$ are determined from the measured depolarization. The magnetic domain size $\delta_\parallel$ is in fact determined by the total magnetic

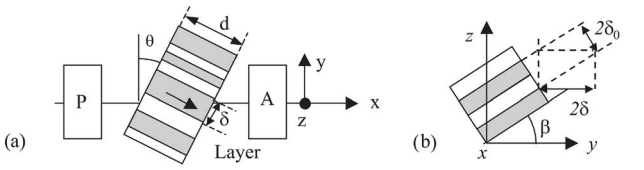

FIG. 3. (a) Sketch of the magnetic layer in the neutron depolarization setup. The polarized beam passes the foil in the x direction, with the polarization directed in the x, y, or z direction by the polarizer P. The polarization component D_z has been analyzed successively in the analyzer A. (b) Sketch of the model with a layered magnetic domain at $\theta=0$, oriented parallel to the x direction and distributed in the yz plane at angle φ with the y axis.

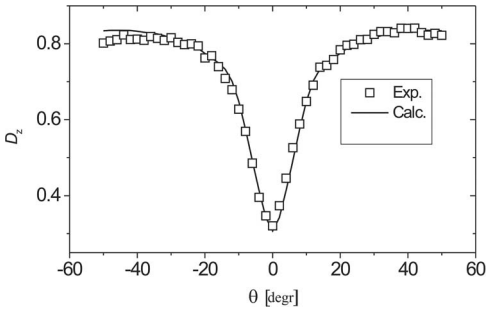

FIG. 4. Measured D_z as a function of the transmission angle θ of the neutron beam (open squares) in a double nickel layer on both sides of a copper sheet. The solid line gives a fit of the data to Eq. (21), with two layers of thickness $d=16.5$ μm, an average domain width $\delta_0=1.8$ μm, and a layer size in the yz plane of about six times δ_0.

cross section ($\Sigma \propto \xi \propto \delta_{\|}$). The average square components in the reduced magnetization $\langle m_i^2 \rangle$ can be directly related to the magnetic texture parameters $\gamma_i=\alpha_{ii}/\xi$, which give additional information on the spread in the orientation of the magnetic domains. From a 3dND experiment, in principle, not more than a mean size of the inhomogeneity in the transmission direction $\delta_{\|}$ and, in addition, the directions of the local magnetization can be determined, with the restriction that $\mu_0 M_s$ and the sample thickness t are known. By varying some external parameters such as the transmission angle, additional information about the inhomogeneity size in the other directions can be obtained.

In magnetic SESANS, in principle, the distribution of the inhomogeneities can be determined, independent of the sample thickness t and the spontaneous magnetic induction $\mu_0 M_s$ from the dependence of the signal on the spin-echo length Z. When t and $\mu_0 M_s$ are known then the size of the inhomogeneities in the beam direction can be determined in absolute numbers from the cross section of the sample that determines the polarization level at $Z \rightarrow \infty$. Both techniques determine some quantities in a different way, but are complementary in the details that can be seen from a sample in study. However, magnetic SESANS is an extension to neutron depolarization, as it also gives information about the size distribution of the inhomogeneity in addition to the average size.

To verify our findings above we have investigated some extreme magnetized samples. We investigated three different samples with a local magnetization confined in the x, y, and z directions. For the x-magnetized sample we used an electrodeposited Ni layer on a copper sheet that appears to create a domain structure that, for 90% of the volume, has its local magnetization perpendicular to the sheet. For the sample with its local magnetization in the $\pm y$ direction, we used an amorphous ribbon under stress in the y direction that appears to give the required domain structure. The same sample was used for the z magnetization by rotating the sample over 90° around the x axis.

A. Angle dependent depolarization experiments on a magnetized layer

The sample was positioned in a polarized beam, as shown in Fig. 3. The magnetization of the domains is directed perpendicular to the layer and coincides with the x direction at $\theta=0$. The layer itself can be rotated about the z direction. The change in polarization caused by such a layer is described by[13]

$$D_z'(\delta,\beta,\theta) = \frac{1}{A_{\delta,\beta}} \sin(A_{\delta,\beta}\varepsilon) + (1-\varepsilon)\cos(A_{\delta,\beta}\varepsilon), \tag{39}$$

where $\varepsilon=(-1)^N(\tan\theta/\eta - N)+1-(-1)^N/2$, with

$$\eta = \delta/[d\cos(\beta)] \text{ and } N = \text{Integer}[\tan(\theta)/\eta],$$
$$A_{\delta_0,\beta} = \frac{\omega\delta}{v\sin(\theta)\cos(\beta)}, \tag{40}$$

which leads to a depolarization component in the z direction of

$$D_z(\delta,\beta_m,\theta) = \int_{\beta_m}^{\pi/2} P(\beta) D_z'(\delta,\beta,\theta)\, d\beta. \tag{41}$$

The quantity $A_{\delta,\beta}$ corresponds to the mean rotation angle of the polarization on passage through one domain and $P(\beta)$ describes the distribution of domain directions as experienced by the neutrons. Figure 3(b) shows that $P(\beta)$ is determined by parallel layers of domains with an orientation φ in the xz plane and that $\delta=\delta_0/\cos(\beta)$ for a flat distribution of β between $\beta_m<\beta<\pi/2$. The minimum β_m in β accounts for the fact that the layers are not flat to infinite y values but have an average length/thickness ratio of about $1/\beta_m$, due to the curvature of the spaghetti structure. In the depolarization experiments this can only be observed in the y direction [Fig. 3(b)]. Figure 4 shows the z component of the polarization measured on the electroplated Ni layer together with a calculated curve when β is averaged over an angle from $\beta_m=0.15$ to $\pi/2$. The fitted depolarization curve shows no sensitivity for a distribution width of δ_0 around the average value of 1.8 μm. A distribution in δ_0 up to 60% full half-width gave a good agreement with the experimental results within the experimental errors.

B. Magnetic SESANS on a double Ni layer

SESANS experiments have been carried out on the same Ni layer to compare these results with the depolarization results and to investigate, together with other uniaxial domain structures, the characteristic properties of magnetic

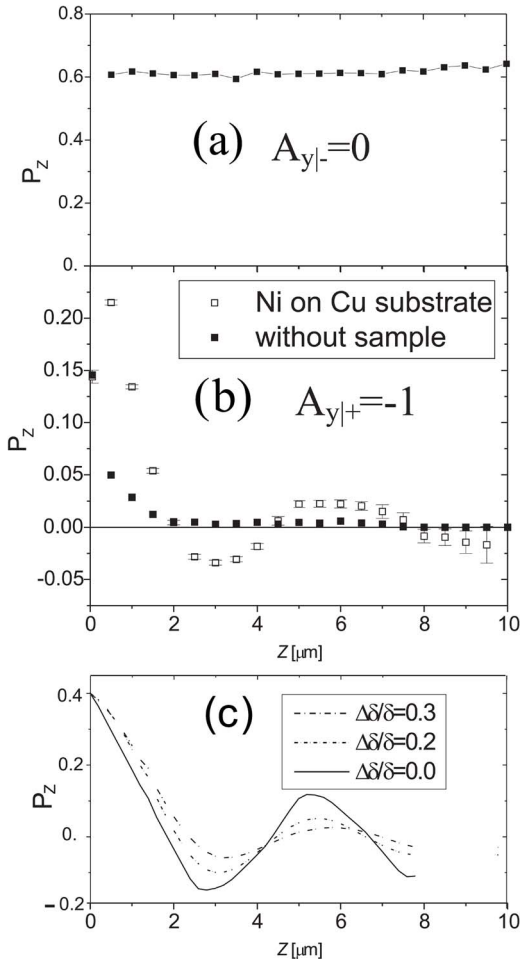

FIG. 5. (a) Measured SESANS signal in the normal spin-echo mode with an instrumental spin flip. (b) Measured SESANS signal without an instrumental spin flip. The magnetic scattering itself causes a spin flip around the x axis according to Fig. 2. The measured polarization P can be directly related to $G_{y|F}(Z)$, with Z determined by the instrumental quantities $\cot(\theta_0)=10$, $\lambda=0.2$ nm, and the magnetic field varying between 0 and 0.15 T. In (a) the magnetic scattering is not echoed ($F=-1$) and leads to a fully depolarized contribution to P, which is the actual depolarization from 1 to 0.6 over the whole Z range. In (b) only the magnetic scattering ($F=+1$) contributes to the echo and should be maximal at $Z=0$, which corresponds to the 40% missing in (a). The signal measured at low Z without a sample has to be attributed to a nonperfect canceling of the nonechoed signal because in this region the total rotation angle is relatively small. In (c) the SESANS signal is calculated with the same distribution of domains as described in Fig. 4 but with different distributions in the domain width as shown in the insert of this figure.

SESANS. Figure 5 shows the experimental results for a precession around the y direction with an instrumental spin flip ($F=-1$) and without ($F=1$).

In the normal spin-echo mode ($F=-1$) we observe in Fig. 5(a) a signal with no Z dependence but with a significant reduction in the polarization to 0.6 of the initial value without the sample (not shown). The constant polarization here reflects the transmission of the unscattered neutrons. The scattered neutrons are fully depolarized, as can be predicted from Eqs. (31) and (42) with $A_{y|-}=0$ and $A_{y|+}=-1$. The reduction in polarization to 60% is caused by the purely magnetic scattering from the domains magnetized in the plus and minus x direction. This magnetic scattering, however, causes a complete depolarization according to Eqs. (29) and (31) when $A_{y|-}=0$. The magnitude 0.4 for the magnetic scattering follows from the depolarization to 0.6 in the mode with $F=-1$. The structure of the magnetic scattering appears when the instrumental spin flip is in the $F=+1$ mode, i.e., $A_{y|+}=-1$, as shown in Fig. 5(b). The polarization of the unscattered beam is here fully damped according to Eqs. (29) and (31), while the magnetic scattering has a full amplitude of $A_{y|+}=-1$. Because we have no z magnetization we only measure the SESANS correlation function $G_{y|-}(Z)$ of the x magnetization. From Fig. 5(b) it is difficult to estimate the value at $Z=0$. The reason for this is that at the lower Z values the admixing of the polarization of the unscattered neutrons, which is not fully damped out, prohibits such a determination [φ in Eq. (29) is not very large]. However, from the results in Fig. 5(a) one may state that $P(0)$ should be 0.4. The results in Fig. 5(b) can be compared with a calculated signal in Fig. 5(c), where the SESANS signal is shown with the same domain geometry of Fig. 4 that was used to interpret the depolarization results in Fig. 3. The calculation was done using Eq. (35), with the model shown and described in Fig. 3(b). However, to fit the SESANS results we needed extra information about the domain size distribution that could not be derived from the depolarization results. Figure 5(c), with a flat distribution of width $\Delta d/d=0.3$ (width at half-height amounts to 0.6) gave about the same damped wave as observed in the measurements. These measurements demonstrate that magnetic SESANS gives essential new information about the distribution of domain sizes that could not be deduced from the neutron depolarization measurements.

To demonstrate the flipping properties of the magnetic scattering, we performed, in addition to the previous experiments on the nickel layer, experiments on the domain structure in an amorphous foil under stress. The latter is characterized by a uniaxial local magnetization parallel to the stress direction.

In Fig. 6(a) the results are shown for the SESANS experiments with a y precession axis and an instrumental spin flip in the $F=-1$ mode. The sample is magnetized in the z direction. This magnetization direction allows only a scattering for $Q_y\neq 0$ and is characterized by $A_{y|-}=0$ and $A_{y|+}=-1$. The contribution for $F=-1$ is fully damped to a constant polarization of about 65% of the unscattered neutrons.

In Fig. 6(c) the results are shown for the same instrumental settings, as in Fig. 6(a), except that the instrumental spin flip has been put in the $F=+1$ mode. In this case the polarization of the unscattered neutrons is fully damped because there is no echo in this mode. The scattered neutrons with $Q_y\neq 0$ underwent a spin flip, and the argument in the cosine of Eq. (34) is zero. As a result, we see a flat Z dependence with an amplitude that corresponds to just the magnetic scattering of about 35%.

In Fig. 6(b) the results are shown for the same instrumental settings, as in Figs. 6(a) and 6(b), but for the sample magnetization rotated into the y direction. We have $A_{y|-}=-1$ and $A_{y|+}=0$. Now we have the interesting case that the magnetic scattering has no extra spin flip but only an extra π rotation (negative sign of $A_{y|-}=-1$) with respect to the unscattered neutrons. This means that the magnetic contribution

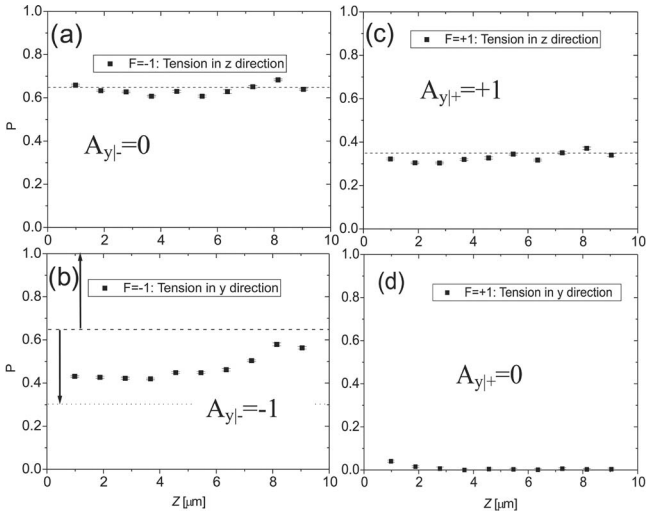

FIG. 6. SESANS measurements with[(a) and (b)] an instrumental spin flip ($F=-1$) and [(c) and(d)] without an instrumental spin flip ($F=+1$). Note the two arrows in (b) indicating the change of sign in the magnetic contribution to the unscattered fraction because of a π phase change. The dashed and dotted lines indicate the levels of the unscattered fraction and the difference of unscattered and magnetic scattered fractions, respectively.

is in antiphase with respect to the unscattered neutrons. So here we already have an amplitude that is equal to the amplitude of the unscattered neutrons diminished with the amplitude of the magnetic scattered neutrons at $Z=0$. In the figure we indicated as dashed and dotted lines the levels of the unscattered neutrons and the difference of unscattered and magnetically scattered neutrons as derived from the previous figures. That the levels do not coincide perfectly with the measurements in this figure must be attributed to experimental errors, such as occur in the π rotation of the scattered neutrons that are very sensitive to the local magnetization directions and the orientation of the precession plane at the sample position. With increasing Z we see a damping of the magnetic contribution as an increase of the total level to about 0.70 of the unscattered neutrons. In Fig. 6(d) all the signals are damped to zero because there is no π flip causing echoing for either of the signals ($A_{y|+}=0$).

VII. DISCUSSION

In the study of magnetic materials it appears that magnetic SESANS gives additional information to the more classical neutron depolarization. The basic difference between SANS (SESANS) and 3dND is that in SANS one determines the domain sizes perpendicular to the transmission direction ($\delta_{\perp}$), while in 3dND one determines the magnetic cross section that is proportional to the average domain size parallel to the transmission direction ($\delta_{\|}$) in the product with the square of the local magnetic induction $\mu_0 M_s$.

In analogy with 3dND where information can be obtained about the local magnetization texture, magnetic SESANS enables one to do a similar job. By measuring successively with the xy, yz, and zx precession planes, the spin-flip properties of the different magnetization components allow for a separation of the different scattering contributions.

The sensitivity ranges of both techniques are fully dependent on the magnetic scattering cross section that both scale with the square of the neutron wavelength and are therefore comparable. When using a neutron wavelength of $\lambda=0.2$ nm, domain size distributions can be studied up to several microns. Selecting the wavelength and the sample thickness, one can optimize the sensitivity for smaller and larger magnetic inhomogeneities. However, where mixed nuclear and magnetic scattering both occur, large differences between the two can cause problems in the determination of the individual terms..

Another point of concern that may affect the interpretation of measurements on large inhomogeneities is the validity of the Born approximation used in the derivation and definition of the SESANS correlation function and the depolarization formula. In the formulation of the SESANS function $G(Z)$ in Eqs. (20)–(22), but also in the derivation of the depolarization formula in Eqs. (11)–(13), we have assumed that the Born approximation (BA) applies, which means that the phase change of the beam over one inhomogeneity is smaller than 1. For very large inhomogenities (larger than 10–20 μm), we arrive at the edge where the BA can be applied without corrections. The validity of the Born approximation can be estimated from the deviation of $\sin(x)/x$ from 1, with x as the phase change over one single inhomogeneity. In our measurements on the Ni layer with a wavelength $\lambda=0.2$ nm the factor $\sin(x)/x$ is larger than 0.9, which demonstrates that the BA is valid. At larger inhomogeneities one has to account for the large phase changes in the inhomogeneity itself.

ACKNOWLEDGMENTS

This research project has been supported in part by the European Commission under the Sixth Framework Programme through the Key Action: Strengthening the European Research Area, Research Infrastructures (Contract No. RII3-CT-2003-505925) and by the INTAS foundation (Grant No. INTAS-03-51-6426). One of the authors (S.G.) thanks RFBR (Grant No. 05-02-16558).

[1] V. F. Sears, *Neutron Optics* (Oxford University Press, New York, 1989).
[2] L. A. Feigin and D. I. Svergun, *Structure Analysis by Small-Angle X-Ray and Neutron Scattering* (Plenum, New York, 1987).
[3] M. Th. Rekveldt, J. Plomp, W. G. Bouwman, W. H. Kraan, S. Grigoriev, and M. Blaauw, Rev. Sci. Instrum. **76**, 033901 (2005).
[4] O. Halpern and T. Holstein, Phys. Rev. **59**, 960 (1941).
[5] S. V. Maleev and V. A. Ruban, Sov. Phys. JETP **31**, 111 (1970).
[6] M. Th. Rekveldt, Z. Phys. **259**, 391 (1973); Nukleonika **24**, 809 (1979).
[7] S. V. Grigoriev, W. H. Kraan, M. Th. Rekveldt, T. V. Kruglov, and W. G. Bouwman, J. Appl. Crystallogr. **39**, 252 (2006).
[8] Y. A. Izyumow and R. P. Ozerov, *Magnetic Neutron Diffraction* (Plenum, New York, 1970), pp. 171–176.
[9] R. Rosman and M. Th. Rekveldt, Z. Phys. B: Condens. Matter **79**, 61 (1990).
[10] M. Th. Rekveldt, W. G. Bouwman, W. H. Kraan, O. Uca, S. V. Grigoriev, K. Habicht, and T. Keller, *Neutron Spin Echo Spectroscopy*, Lecture Notes in Physics, edited by F. Mezei, C. Pappas, and T. Gutberlet (Springer, Berlin, 2003), pp. 87–99.
[11] M. Th. Rekveldt, W. G. Bouwman, W. H. Kraan, O. Uca, S. V. Grigoriev, and R. Kreuger, *Neutron Spin Echo Spectroscopy*, Lecture Notes in Physics, edited by F. Mezei, C. Pappas, and T. Gutberlet (Springer, Berlin, 2003), pp. 100–115.
[12] T. Krouglov, I. M. de Schepper, W. G. Bouwman, and M. Th. Rekveldt, J. Appl. Crystallogr. **36**, 117 (2003).
[13] W. H. Kraan and M. Th. Rekveldt, J. Magn. Magn. Mater. **5**, 247 (1977).